

Synthesis, Characterization and Photocatalytic Performance of N-Doped MgO for Prospective Packaging Use

Annalisa Pace^{*,a}, Francesca Di Fiore^a, Vincenzo Vaiano^b, Vincenzo Venditto^a, Olga Sacco^a

^a University of Salerno, Department of Chemistry and Biology "A. Zambelli", Via Giovanni Paolo II, 132, Fisciano (SA), Italy

^b University of Salerno, Department of Industrial Engineering, Via Giovanni Paolo II, 132, 84084 Fisciano (SA)

apace@unisa.it

In this study, magnesium oxide (MgO) and nitrogen-doped magnesium oxide (N-MgO) were synthesized using different precursors, such as magnesium sulfate (MgSO₄) and magnesium acetate (Mg(CH₃COO)₂), through various synthetic procedures. Thanks to its biocompatibility and antimicrobial, antifungal, and antiviral activity, MgO is considered a promising candidate for active food packaging applications. However, since MgO is a wide-bandgap semiconductor that is only active under UV light, nitrogen doping was introduced to extend its photocatalytic activity into the visible light range. XRD and FTIR analyses confirmed the presence of the cubic MgO phase and revealed structural changes induced by nitrogen doping. Photodegradation tests on a probe molecule (methylene blue) showed that the N-MgO material achieved an efficiency of 97% under visible light, highlighting a significant enhancement in photocatalytic properties compared to undoped MgO

1. Introduction

Metal oxide, such as TiO₂, ZnO, MgO, and SnO₂, possess distinctive properties—including thermal stability, reactivity, and biocompatibility—that make them suitable for applications in optics, sensing, electronics and photocatalysis (Farani et al., 2023). MgO is particularly valued for its eco-friendly nature, non-toxicity, and its ability to generate reactive oxygen species (ROS), which provide antiparasitic and antimicrobial properties without the need for light activation. In contrast, TiO₂ requires light activation to exhibit antibacterial effects, while ZnO, although effective, presents cytotoxicity issues that limit its use in food-related applications (Karuppan Perumal et al., 2025). These characteristics support the use of MgO in the food industry, where it is approved as an additive (E530) by both the EFSA (European Food Safety Authority) and the FDA (U.S. Food and Drug Administration), including in nanoscale form (Yang et al., 2024), thus making it a promising candidate for food packaging applications. However, the semiconducting nature of MgO, characterized by a wide band gap, limits its activity only under UV light, reducing its effectiveness as a photocatalyst under visible light. Doping with non-metal elements such as sulfur (S), phosphorus (P), and carbon (C) can reduce the band gap and enhance absorption in the visible region (Akbari et al., 2022). Despite some investigations on these elements, studies on nitrogen doping of MgO remain limited. Therefore, this study aims to investigate nitrogen doping to improve catalytic performance. Two approaches were tested: in situ doping during sol–gel synthesis and post-synthesis doping via calcination in a nitrogen atmosphere. The resulting materials were characterized and evaluated for their ability to degrade methylene blue under visible light irradiation.

2. Experimental

2.1 Synthesis procedure of MgO particles

The reagents used include potassium hydroxide (KOH, pellets, VWR Chemicals), magnesium acetate tetrahydrate (Mg(CH₃COO)₂·4H₂O, Carlo Erba), magnesium sulfate heptahydrate (MgSO₄·7H₂O, 99.5%, Sigma-Aldrich), urea (CH₄N₂O, Sigma-Aldrich) and ammonia aqueous solution (30 wt%, Carlo Erba).

All compounds were used without further purification, and the solutions were prepared using deionized water (18 M Ω -cm).

In this study, two different doping methods were explored, leading to the synthesis of four magnesium oxide-samples. Different precursors and synthesis procedures were used in order to evaluate which doping method more effectively modifies the photocatalytic activity under visible light.

The samples synthesized were undoped MgO (A), N-MgO (A), undoped MgO (B), and N-MgO (B)

2.1.1 Procedure for Method A

Undoped MgO (A) were prepared by dissolving 5 g of MgSO₄·7H₂O in 250 mL of deionized water under magnetic stirring, followed by the dropwise addition of a 0.1 M potassium hydroxide (KOH) solution.

The resulting mixture was refluxed at 100 °C under continuous stirring for 4 h. Afterward, the suspension was kept stirring at room temperature for an additional 12 h. The precipitate formed was recovered by centrifugation, washed several times with deionized water to remove residual ions and impurities.

The dried solid was then finely ground using a mortar and pestle. It was subsequently calcined in a muffle furnace in air at 550 °C for 2 hours, with a heating rate of 10 °C/min.

The preparation of N-MgO (A) involved the use of the same precursors and synthesis procedure. However, the calcination was performed in a N₂ atmosphere muffle furnace at 550 °C for 2 hours, with a heating rate of 10 °C/min.

2.1.2 Procedure for Method B

Undoped MgO (B) was synthesized by dissolving 5 g of magnesium acetate in 250 mL of deionized water and stirring the solution for 30 minutes.

Subsequently, a 0.1 M KOH solution was added, and the mixture was stirred for 18 hours.

The prepared gel was centrifuged and washed with deionized water several times.

The washed gel was dried in an oven (100°C) and subsequently ground into a fine powder.

Finally, the as-prepared product was calcined at 350°C for 2h at a heating rate of 10°C/min

N-MgO (B) were obtained via a sol-gel method similar to that used for undoped MgO, with variations in precursors and operating conditions. Specifically, a 2:1 molar ratio of urea to magnesium was used, and ammonia solution was added as the basic agent until the pH reached between 9-10, maintaining the system under stirring at room temperature for 18 hours.

The resulting gel was centrifuged, washed, dried in an oven, and then calcined under the same conditions as the undoped MgO (B).

2.2 Characterization techniques

The crystalline phase of the samples was determined by X-ray diffraction using a Bruker D8 Advance diffractometer performed in the 2 θ range from 3° to 90°, using copper (Cu) as the anode and K α ₁ radiation (λ =1.5418 Å). The average crystallite sizes of all the prepared samples are calculated by Debye-Scherrer's method as shown in Eq.(1)

$$D = \frac{k\lambda}{\beta \cos \theta} \quad (1)$$

Where D is the crystallite size, λ = 1.5418 Å is the wavelength of the Cu-K α X-ray source, k is the Scherrer shape constant (0.89), β is the full width at half maximum intensity (FWHM), and θ is the peak position. The chemical bonds were identified by Fourier Transform Infrared Spectroscopy (FTIR) using a Vertex 70 spectrometer from Bruker, equipped with a deuterated triglycine sulphate (DTGS) detector and a Ge/KBr beam splitter, operating in the frequency range of 390–3900 cm⁻¹.

2.3 Photocatalytic activity tests

A 5 mg·L⁻¹ aqueous solution of methylene blue (MB) was prepared by dissolving 1.25 mg of the dye in 250 mL of Milli-Q water.

Photocatalytic tests were conducted in a Pyrex batch reactor under visible light using four Vis lamps (Philips, nominal power: 8 W, with emission in the range 400–750 nm) placed at a distance of 10 cm from the reactor's external surface, in order to irradiate the solution volume uniformly. For the tests, a suspension containing 100 mL of the dye solution and 1.0 g·L⁻¹ of catalyst was prepared and kept in the dark for 2 hours to reach the adsorption/desorption equilibrium. Afterward the lamps were switched on for 180 minutes.

During irradiation, 1.5 mL aliquots were collected at regular time intervals, centrifuged, and analyzed to determine the residual concentration of methylene blue. Absorbance at λ = 664 nm was measured using an Agilent Varian Cary 50 Probe Uv-vis spectrophotometer.

3. Results and Discussion

3.1 Characterization of the samples

The XRD spectra of the undoped MgO (A) and N-MgO (A) and the undoped MgO (B) and N-MgO (B) samples are shown in Figure 1a and Figure 2, respectively.

All samples exhibit the main diffraction peaks corresponding to the crystalline phase of MgO with a cubic rock-salt structure (JCPDS card no. 01-075-0447)

Figure 1b shows a slight shift toward lower diffraction angles in the peaks of the N-MgO (A) sample.

The observed shift could probably be attributed to the modification of the lattice parameters induced by the incorporation of the dopant. The analysis of the average crystallite size, calculated using the Debye-Scherrer formula Eq(1), shows a significant reduction of D in the N-MgO (A) sample (4,64 nm) compared to the undoped MgO (A) sample (9,94 nm).

This indicates that nitrogen doping inhibits crystal growth, promoting the formation of smaller crystallites. This effect can be attributed to the introduction of defects or lattice strains induced by the dopant, which reduce the overall crystallinity of the material.

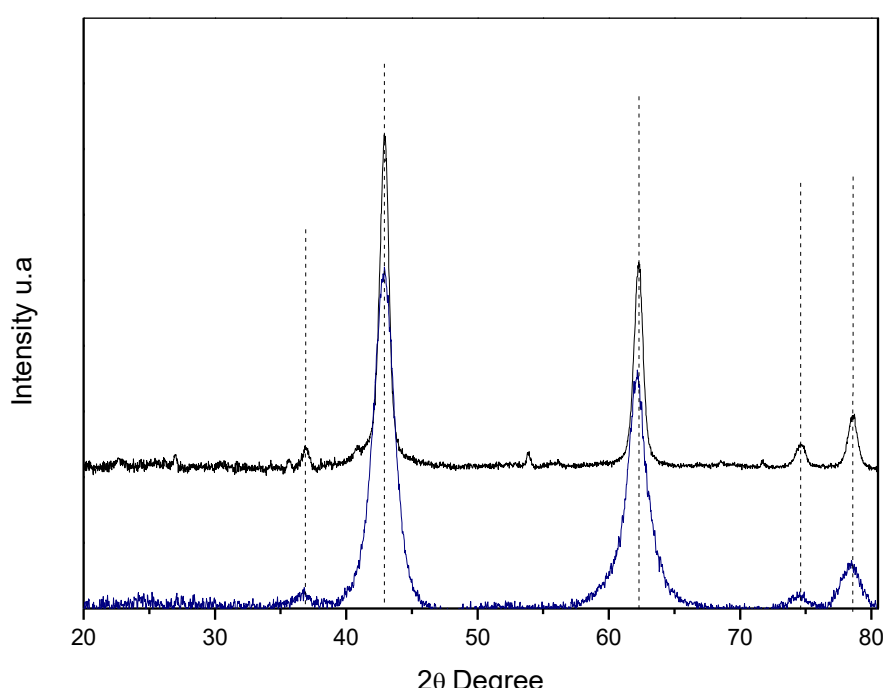


Figure 1: a) XRD analysis of undoped MgO (A) and N-MgO (A) b) Shift of the (200) XRD peak of N-MgO (A)

Figure 2 illustrates the XRD patterns of the undoped MgO (B) and N-MgO (B) samples, no peak shifts are observed, and the crystallite size (D) is similar, approximately 11 nm and 12 nm respectively.

However, after normalization to the (200) reflection, the $I(hkl)/I(200)$ ratios corresponding to the (111), (220), (222), and (311) planes are reduced in the doped sample compared to undoped MgO (B), likely due to the presence of inclusions or defects introduced by the dopant.

The FTIR spectra of the samples undoped MgO (A) and N-MgO(A), shown in Figure 3a, and of undoped MgO (B) and N-MgO (B), shown in Figure 3b, were recorded on pellets obtained by finely grinding the synthesized samples with anhydrous potassium bromide (KBr) and subsequently pressed.

The spectra reveal a broad band around 3600 cm^{-1} is attributed to the stretching vibration of hydroxyl groups ($-\text{OH}$), while a band at approximately $1630\text{--}1640\text{ cm}^{-1}$ corresponds to the bending vibration of water molecules (H-O-H) physically adsorbed on the surface of the samples.

The signal at 854 cm^{-1} is indicative of the cubic phase of MgO, while the band at around 473 cm^{-1} is associated with the stretching vibration of the Mg-O bond as reported by (Yadav et al. 2022)

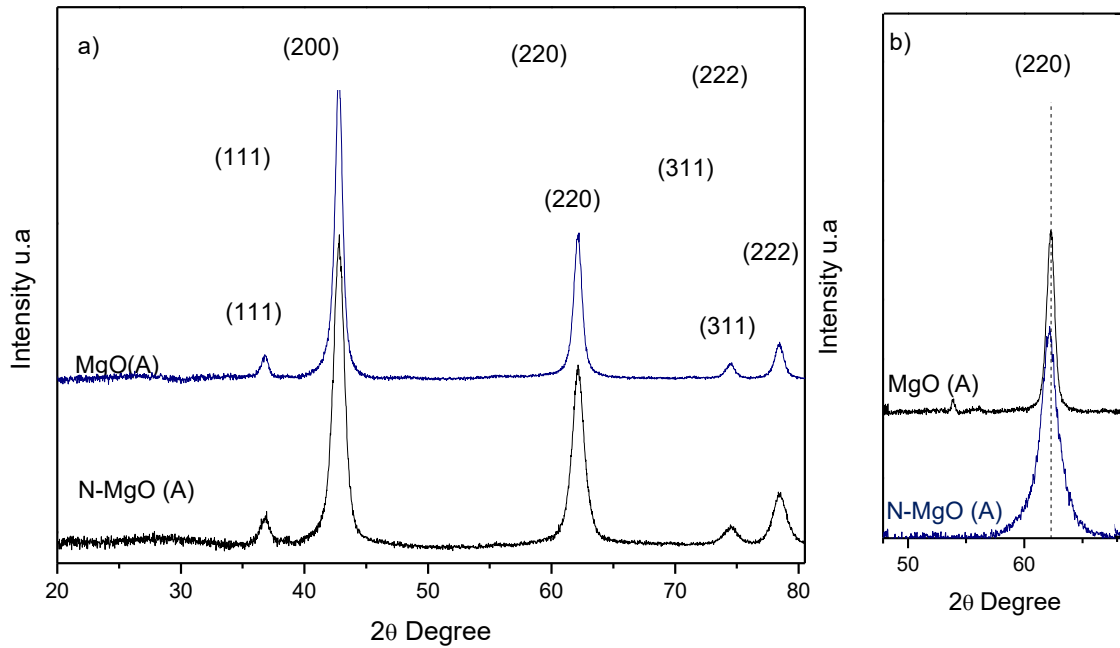


Figure 2: XRD analysis of undoped MgO (B) and N-MgO (B)

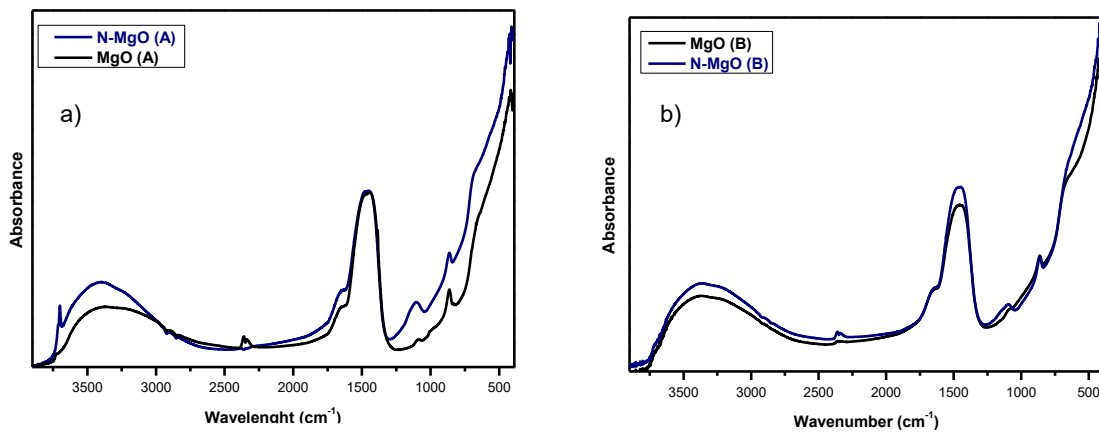


Figure 3: FTIR samples a) undoped MgO (A) and N-MgO (A) b) undoped MgO (B) and N-MgO (B)

3.2 Photocatalytic activity tests

The photocatalytic activity of undoped MgO (A), N-MgO (A), undoped MgO (B), and N-MgO (B) was evaluated under visible light using methylene blue (MB) as a probe molecule representative of an organic pollutant. As shown in Figure 4, undoped MgO (A) degraded only 18% of methylene blue after 180 minutes - comparable to photolysis- indicating poor activity in the visible range. In contrast N-MgO (A) showed significantly improved degradation (~48%) confirming enhanced photocatalytic activity due to doping-induced electronic structure modification. N-MgO (B), synthesized using urea and ammonia as nitrogen sources, exhibited the highest efficiency (~97%), far exceeding the corresponding undoped MgO (B) (~50%) as observed in Figure 5. The degradation efficiency of the target organic pollutant MB was calculated for synthesized samples using the following equation Eq(2):

$$\text{Degradation \%} = \left[\frac{C_0 - C}{C_0} \right] \cdot 100 \quad (2)$$

where C_0 is the final dark dye concentration blue and C is the dye concentration at time t . The resulting degradation values are summarized in Table 1.

Table 1: Summary of degradation efficiencies and kinetic parameters of the prepared photocatalysts.

Sample	k (min ⁻¹)	R ²	Degradation efficiency%
MgO (A)	0.001	0.9552	18
N-MgO (A)	0.0035	0.9976	48
MgO (B)	0.0034	0.9758	50
N-MgO (B)	0.017	0.9842	97

Additionally, to quantitatively evaluate the photocatalytic activity exhibited by the different samples, the apparent pseudo-first-order rate constant k was determined using the following equation Eq(3):

$$-\ln\left(\frac{C}{C_0}\right) = kt \quad (3)$$

The k value (min⁻¹) was obtained from the slope of the straight line resulting from the plot of $-\ln(C/C_0)$ versus irradiation time t . The calculated k values for all the samples are also reported in Table 1.

Overall N-MgO (B) outperforms N-MgO (A), suggesting that the urea–ammonia doping method is more effective. XRD data support that nitrogen incorporation differs between methods, indicating distinct doping mechanisms based on the synthesis route.

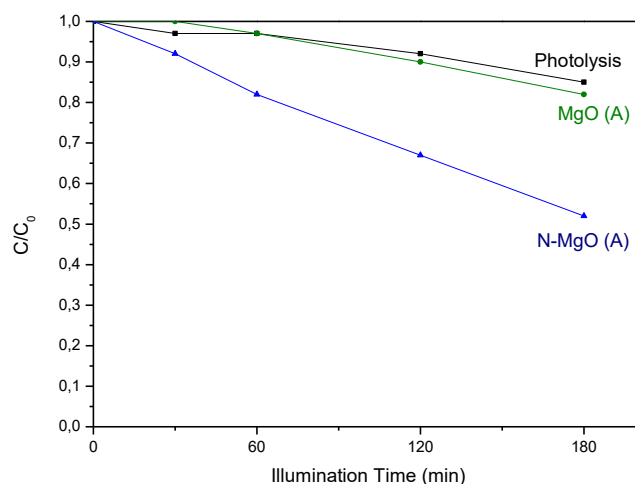


Figure 4: Photocatalytic degradation of MB (C/C_0) over time under visible light for undoped MgO (A), N-MgO (A) samples.

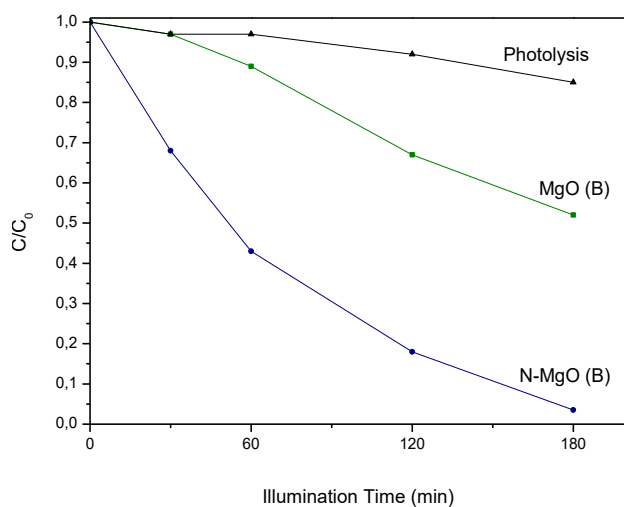


Figure.5 Photocatalytic degradation of MB (C/C_0) over time under visible light for undoped MgO (B), N-MgO (B) samples.

4. Conclusions

In this study, two nitrogen doping methods were evaluated to improve the photocatalytic activity of MgO under visible light: in situ doping during the sol-gel synthesis, using ammonia and urea as nitrogen sources, and post-synthesis doping by calcination in a nitrogen atmosphere.

X-ray diffraction analysis revealed, in the N-MgO (A) sample obtained by the post-synthesis method, a slight peak shift compared to pure MgO, indicative of a slight lattice deformation due to nitrogen incorporation.

This structural modification correlates with an improved degradation of methylene blue (MB).

Conversely, the use of nitrogen-containing reagents as nitrogen sources resulted in significantly higher MB degradation (97%) without causing noticeable shifts in the crystalline structure peaks, likely due to the presence of inclusions or defects introduced by the dopant.

References

- Akbaria S., Moussavia G., Deckera J., Marind M.L., Boscad F., Giannakisa S., 2022, Superior visible light-mediated catalytic activity of a novel N-doped, Fe₃O₄-incorporating MgO nanosheet in presence of PMS: Imidacloprid degradation and implications on simultaneous bacterial inactivation, *Applied Catalysis B: Environmental*, 317, 121732, doi:10.1016/j.apcatb.2022.121732.
- Farani M.R., Farsadrooh M., Zare I., Gholami A., Akhavan O. (2023). Green synthesis of magnesium oxide nanoparticles and nanocomposites for photocatalytic antimicrobial, antibiofilm and antifungal applications. *Catalysts*, 13(4), 642. doi:10.3390/catal13040642.
- Karuppan Perumal M., Rajasekaran M.B.S., Renuka R.R., Samrot A.V., Nagarajan M., 2025, Zinc oxide nanoparticles and their nanocomposites as an imperative coating for smart food packaging, *Applied Food Research*, 5(1), 100849, ISSN 2772-5022, doi:10.1016/j.afres.2025.100849.
- Yang J., Wang X., Khan M.R., Hammouda G.A., Alam P., Meng L., Zhang Z., Zhang W. (2024). New opportunities and advances in magnesium oxide (MgO) nanoparticles in biopolymeric food packaging films. *Sustainable Materials and Technologies*, 40, e00976. doi:10.1016/j.susmat.2024.e00976.
- Yadav P., Saini R., Bhaduri A. (2022). Facile synthesis of MgO nanoparticles for effective degradation of organic dyes. *Environmental Science and Pollution Research*, 30(28), 71439–71453. doi:10.1007/s11356-022-21925-0.